

Hyperspectral Nanoscale Imaging on Dielectric Substrates with Coaxial Optical Antenna Scan Probes.

Alexander Weber-Bargioni,^{*,†} Adam Schwartzberg,^{†,⊥} Matteo Cornaglia,^{†,||} Ariel Ismach,[†] Jeffrey J. Urban,[†] YuanJie Pang,[‡] Reuven Gordon,[‡] Jeffrey Bokor,^{†,§} Miquel B. Salmeron,[†] D. Frank Ogletree,[†] Paul Ashby,[†] Stefano Cabrini,^{*,†} and P. James Schuck^{*,†}

[†]Molecular Foundry, Lawrence Berkeley National Laboratory, One Cyclotron Road, Berkeley, California 94720, United States

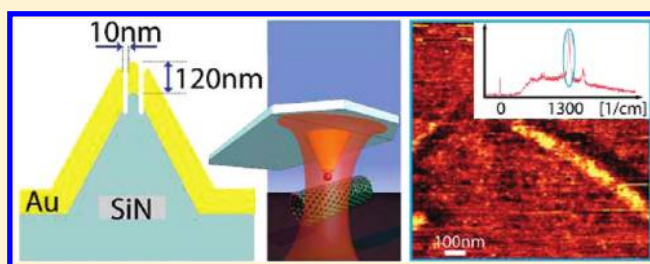
[‡]Department of Electrical and Computer Engineering, University of Victoria, EOW 448, 3800 Finnerty Road, Victoria, British Columbia V8P 5C2, Canada

[§]EECS Department, UC Berkeley, 253 Cory Hall MC No. 1770, Berkeley California 94720-1770, United States

S Supporting Information

ABSTRACT: We have demonstrated hyperspectral tip-enhanced Raman imaging on dielectric substrates using linearly polarized light and nanofabricated coaxial antenna tips. A full Raman spectrum was acquired at each pixel of a 256 by 256 pixel contact-mode atomic force microscope image of carbon nanotubes grown on a fused silica microscope coverslip, allowing D and G mode intensity and D-mode peak shifts to be measured with ~ 20 nm spatial resolution. Tip enhancement was sufficient to acquire useful Raman spectra in 50–100 ms. Coaxial scan probes combine the efficiency and enhanced, ultralocalized optical fields of plasmonically coupled antennae with the superior topographical imaging properties of sharp metal tips. The yield of the coaxial tip fabrication process is close to 100%, and the tips are sufficiently durable to support hours of contact-mode force microscope imaging. Our coaxial probes avoid the limitations associated with the “gap-mode” imaging geometry used in most tip-enhanced Raman studies to date, where a sharp metal tip is held ~ 1 nm above a metallic substrate with the sample located in the gap.

KEYWORDS: Tip-enhanced Raman spectroscopy (TERS), near-field chemical imaging, hyperspectral imaging, nano-optics, plasmonics, optical antenna



A major nanoscience goal is to unlock previously inaccessible physics and dynamics within nanoscale systems by combining the efficient nanoscale field confinement/optical resolution (~ 10 nm) of optical antennae and the ultrafast temporal resolution (fs) inherent in optical studies with the capabilities of modern scanning probe techniques.¹ Here we report on a significant step toward this goal using a novel nanofabricated coaxial antenna tip capable of recording useful Raman spectra in ~ 50 ms to acquire 256 by 256 pixel images on dielectric substrates with a full spectrum at each pixel.

Though many possible optical antenna designs exist,^{2–19} by far the most promising for near-field imaging purposes use plasmonically coupled structures.^{20–23} These types of antennae take advantage of the ultraenhanced and localized fields created around the nanogaps or crevices between constituent substructures and are responsible for the largest reported scattering and fluorescence signal enhancements to date (e.g., single-molecule surface-enhanced Raman scattering).^{24,25} This has led to near-field imaging spectroscopy methods based on the so-called “gap mode” geometry, where a sharp metal tip is held ~ 1 nm above a metallic substrate (with the sample located in the gap), effectively forming a vertically oriented coupled dipole- or bowtie-like plasmonic antenna.^{26–31} Recently, researchers have used the large field enhancements inherent in this

geometry for full spectroscopic imaging of molecular and polymer layers, collecting a Raman spectrum at each image pixel with subsecond integration times.³⁰ This geometry, however, is rather limiting. First, it requires a metallic substrate and a very small tip–substrate gap, meaning only very thin samples (e.g., molecules) can be investigated, precluding many classes of nanoscale structures and devices. Second, highest enhancements result only when the light is polarized in the “z” direction normal to the sample surface, restricting one of the most useful variable parameters in Raman studies, the probed polarization.

To avoid these constraints, we and others have fabricated dipolelike optical antennae on scan probes, effectively creating the nanogap directly on the tip, allowing for ultrahigh enhancement without the need for metallic substrates and “gap-mode” experimental geometries.^{32,33} Unfortunately, experiments based on this type of scan probe had themselves been limited by a lack of reproducible tip fabrication techniques. But this issue has been recently overcome,³³ and we have used these novel fabrication

Received: November 29, 2010

Revised: January 7, 2011

Published: January 24, 2011

methods to create reproducible bowtie tips that yield repeatable tip-enhanced Raman scattering (TERS) signals similar to those obtained with the gap-mode geometry.^{33,34} Bowtie-based scan probes, however, also have a downside; namely, their relatively flat structure results in comparatively poor topographic imaging qualities and large tip-sample interaction forces.

This has led us to create a new generation of probes built on the coaxial (coax) plasmonic antennae concept. A coax aperture can be thought of as a metal-insulator-metal slit or antenna aperture wrapped back onto itself, yielding low-loss propagation of optical-frequency modes.^{35–38} Recent simulations have suggested that the optical coax geometry can be relatively broadband and efficient at coupling to far-field radiation.^{35,36,39} By fabricating the center conductor with a tapered end, a coax-based probe combines the advantages of plasmonically coupled antennae (polarization flexibility; larger fields) with sharp tips, and with the additional potential benefit of back-illumination (transmission mode) of the coax tip for virtually “background-free” imaging.^{40,41}

Coax tips were fabricated by depositing a 2 nm Ti adhesion layer followed by 120 nm of Au onto commercial (NanoSensors) SiN contact-mode atomic force microscope (AFM) cantilevers. A focused ion beam (FIB) lithography system (Zeiss XB1540) operating at 1 pA beam current and ~ 12 nm resolution was used to mill an annular gap around a 65 nm central pin to create the coax structure. To ensure maximum coupling between outer and inner parts of the coaxial structure, we kept the insulating gap constant and as small as possible (15 to 18 nm, i.e., significantly subwavelength). It is important to note that the FIB fabrication process induces some curvature and tapering of the central pin (see Figure 1d), which is desirable for AFM imaging.

Our tip geometry was determined by fabricating 40, 65, and 160 nm coax test structures with a constant 15 to 18 nm gap in a similar Au/Ti film on a flat glass coverslip (Figure 1a). These structures were characterized theoretically by finite-difference time-domain (FDTD) simulation and experimentally by illumination with white light incident on the air side of the sample and collection of the far-field transmitted spectra using a spectrometer and a liquid nitrogen-cooled charge coupled device (CCD) camera (See Figure 1 and Supporting Information). Typical source- and background-corrected spectra are shown in Figure 1a–c. The respective measured resonant frequencies were 555 ± 2 , 602 ± 3 , and 672 ± 2 nm averaged over 16 structures for the small, medium, and large pin diameters. The details on the resonance fitting are described in the Supporting Information. A 65 nm coax pin diameter was chosen for the tip coax as this gave a good match to the 633 nm HeNe laser line used for the Raman imaging experiments. Furthermore, we also determined that the coaxial antennae maintain far-field polarization in transmission, which will be described in detail in a future work.

Optical coax properties are strongly dependent on structure geometry. De Waele et al. determined the coaxial waveguide's dependence on the length of the coaxial structure,^{39,42} showing superenhanced resonant transmission. Others have simulated coaxial openings for a variety of film thicknesses and determined the dependence on inner pin diameter in the visible regime for perfect electrical conductor (PEC) thicknesses on the order of 100 nm.³⁵

It is important to note that linearly polarized light excites the first order mode for a symmetric coax with a perfectly cylindrical center pin (flat top and bottom surfaces), as the lowest order

mode is not dipole active due to symmetry (the lowest order mode could alternatively be excited by radially polarized or z-polarized light). This is expected to create two localized hot spots at the end of the coax along the polarization direction.^{36,39} We have attempted to create a more singular primary localized field volume by tapering⁴³ and rounding the ends of our coax center pins, which also aids AFM imaging performance. In practice, our Raman images are consistent with a single (vs double) near-field spot signature as shown below. Besides the tapered end, this may also be due to one hot spot being closer to the sample when the AFM tip contacts the surface, or to eccentricity or asymmetry in the coax structure resulting from the nanofabrication process that leads to one dominant hot spot.

Raman imaging was performed using a modified WITec near-field scanning optical microscope (NSOM). The tips were mounted to the microscope's AFM attachment and approached to the sample in contact mode. The 980 nm laser used for AFM deflection sensing was focused on the cantilever through a 20 \times objective above the sample. The coax tips were excited through the fused silica substrate using a linearly polarized HeNe laser focused by a 100 \times 1.4 NA oil objective. The scattered Raman light was collected through the same objective and directed onto either a grating spectrometer with a thermoelectrically cooled CCD camera or a photo multiplier tube (PMT) using a dichroic mirror and long-pass filter. The dichroic rejected scattered light within 400 cm^{-1} of the laser line, preventing the observation of the carbon nanotube (CNT) radial breathing modes. To obtain a near-field signal, the laser (100 μW) was focused on the sample surface, then the tip was moved into the laser focus. The signal was optimized by scanning the laser over the tip apex with a 2D galvanometer (Thorlabs) while recording the Au photoluminescence (PL) signal on the PMT, then placing the laser focus at the position of maximum PL.

Though not possible with our current experimental setup, we note that another major advantage of the coax antenna probes is the ability to excite the antenna through the back of the probe, yielding essentially background-free near-field spectroscopic imaging since only the local optical fields from the antenna excite the sample.

We demonstrated the spectroscopic imaging capabilities of our coaxial tips by imaging carbon nanotubes that were grown directly on fused silica coverslips via CVD using ferritin protein (horse spleen ferritin, Sigma) as a precursor of monodisperse Fe catalyst nanoparticles, as previously^{44,45} reported. CNTs have been investigated extensively via near-field optical spectroscopy^{46–49} and are therefore an ideal test sample. Figure 2a shows a topographic AFM scan acquired with a coax antenna probe. The lateral resolution is on the order of 20 nm, consistent with the radius of curvature of the central coax pin. On the basis of several line scans over the sample, many of the CNT structures appear to be either multiwall CNTs or single wall CNT bundles.

The sample was then positioned so that the tip was placed on a CNT (marker in Figure 2a) and the Raman spectrum was recorded (Figure 2b). The 10 s long spectrum clearly shows the D and G modes at 1308 and 1586 wave numbers along with a PL background originating from the Au antenna. The D- to G-mode intensity ratio was ~ 4.5 . The AFM tip was then retracted to take a far-field confocal spectrum (Figure 2c) of the same area. The spectrum was integrated 12 times longer to achieve a comparable G-mode signal. In confocal mode, the D/G mode ratio was ~ 1 . The increase in the D/G mode ratio for the tip-enhanced spectrum could be caused by localized strain on the CNT induced by the tip

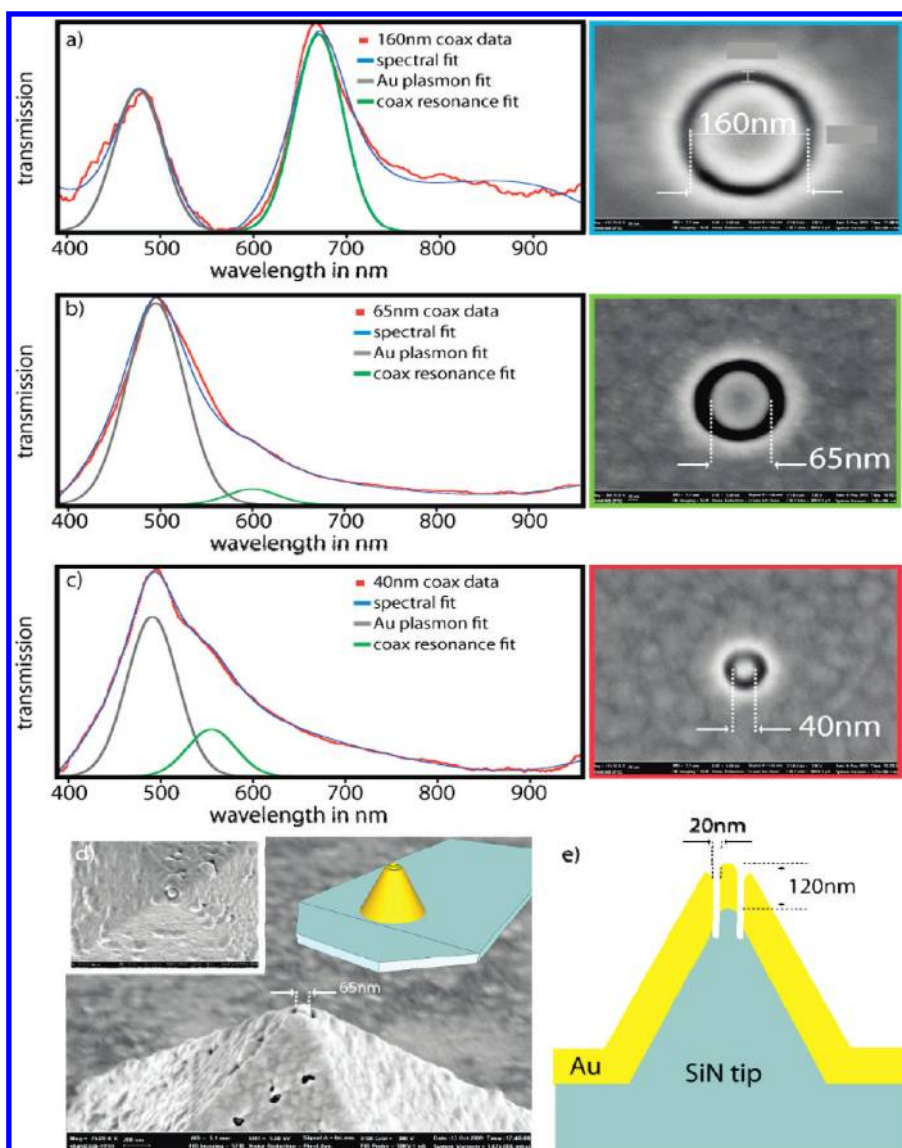


Figure 1. Coaxial optical antennae. (a–c) Three optical coaxial antenna structures fabricated via focused ion beam milling in a 120 nm thick Au film. The antennae are comprised of three different central pin diameters (160, 65, and 40 nm) leading to three different optical resonances. To highlight the antenna resonances, the spectra were fitted with two Gaussians: one for the Au plasmon resonance (gray) and one for the antenna resonance (green). A model and an actual coaxial antenna incorporated on the end of a Scanning Probe Tip are shown in (d) and the cross-section of the coaxial scan probe is represented in (e).

in contact mode. Yano et al. observed an intensity increase and position shift of the G-mode when applying pressure using a sharp metal tip as their near-field probe.⁴⁹ In contrast we observed variations in the D-mode intensity and no detectable peak shifts. We tested various tips and exerted different tip forces on the sample but the intensity of the G-mode was not affected within our experimental resolution. This discrepancy may be related to the different polarizations of the excitation light for the two types of tips (mostly in-plane vs z-polarized), though further studies will be required for better understanding.

Because of the load-dependent D-mode intensity variations, we choose to use the G-mode intensity to compare tip-enhanced and confocal Raman intensity. The data shown here give a G-mode enhancement of 17 (D-mode enhancement 64). We note that there are no area or volume correction factors used in obtaining this number because of uncertainties in active area

estimates and the corresponding controversial estimates of “true” field enhancement; that is, this is the most conservative calculation of enhancement (and the one that ultimately matters most). We tested 8 engineered coax tips, which all showed a G-mode signal enhancement between 12 and 25, which compares favorably to enhancements reported in the literature for sharp tips,^{48,50–54} but with the advantage of being fabricated reproducibly with a distinct optical resonance. We stress that the nanofabricated tip yield approaches 100%; all of the tips that look good in post-FIB SEM images demonstrated significant Raman enhancement. The coax tips were also sufficiently durable to support many hours of contact-mode imaging.

Increasing the laser power after the objective to 150 μW led to satisfactory signal-to-noise ratios in the Raman spectra for integration times as low as 50 ms, enabling practical Raman mapping on dielectric substrates. We were able to take a full

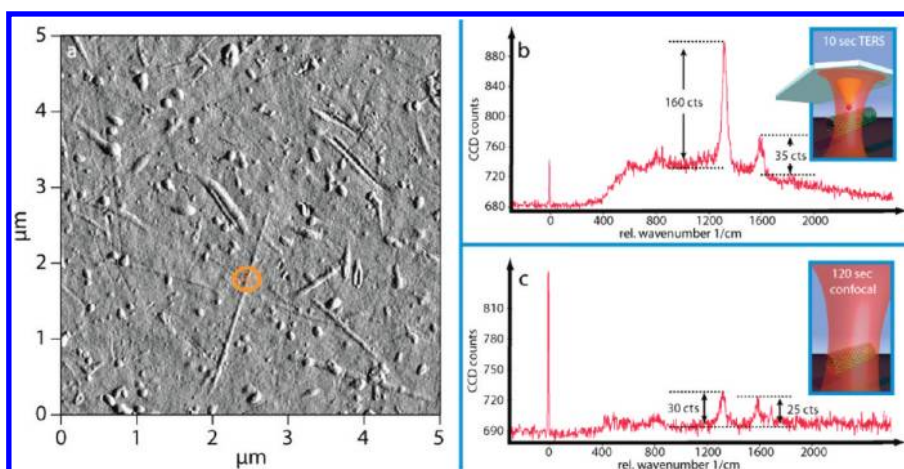


Figure 2. Tip-enhanced Raman spectroscopy on CNTs. (a) Topographic error-signal image of CNTs grown on a fused silica coverslip acquired with the coaxial antenna scanning probe. (b) Tip-enhanced Raman spectrum of the CNT taken at the marked position in (a), integrated over 10 s. (c) Confocal Raman spectrum at the equivalent position. An integration time of 120 s was necessary to achieve a similar G-mode signal.

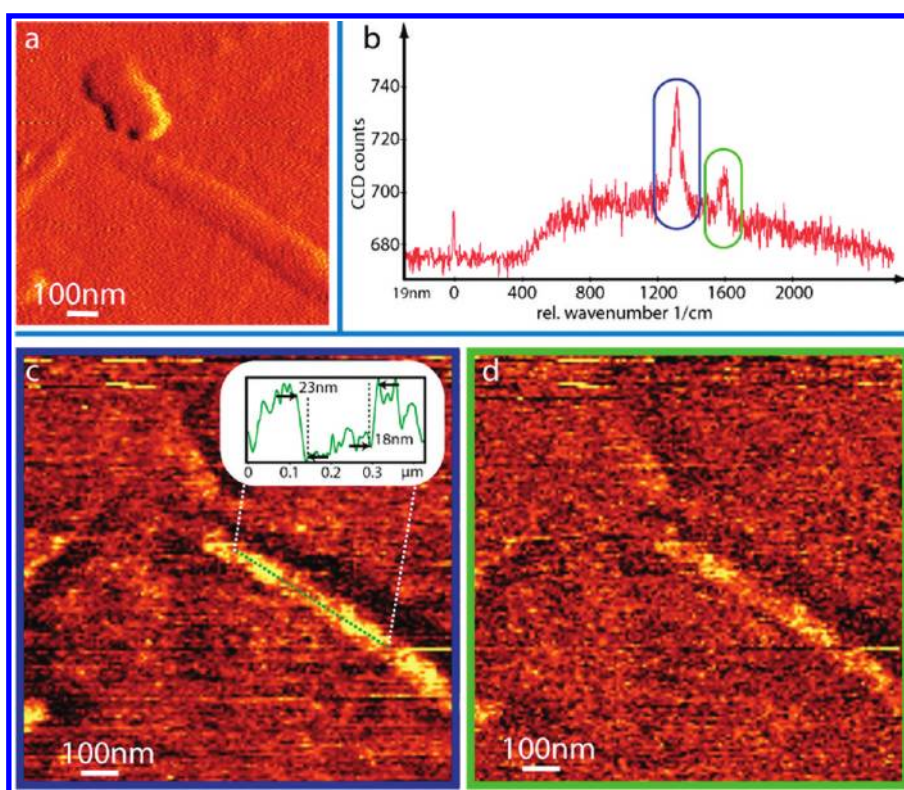


Figure 3. Raman spectral mapping of CNTs. (a) Topography of mapped region (error signal). (b) Example of 0.1 s Raman spectrum which was taken at each pixel. D and G peaks are shown with a blue and green circle, respectively. (c,d) The corresponding intensity maps of the D and G peaks. The inset in (c) is a line-scan demonstrating the optical resolution along the CNT structure. We additionally observed polarization dependence for the imaging performance, which we will report on in a following publication.

Raman Spectrum at each pixel of a near-field imaging scan. While performing a slow $1.5 \mu\text{m}$ by $1.5 \mu\text{m}$ AFM scan over our sample (see Figure 3a topography image), spectra were acquired at each of the 256 by 256 pixels, allowing the detection of small variations in the sample chemistry and composition reflected by small changes in peak positions and intensities. A typical 0.1 s spectrum over the CNTs is shown in figure 3b.

Spectral maps were generated by subtracting the PL background and integrating the Raman peaks from 1250 to

1350 cm^{-1} for the D-band (see Figure 3c) and from 1550 to 1650 cm^{-1} for the G-band (see Figure 3d). The D-mode map, related to the CNT defect density, shows rich detail and strong local variation in intensity, in principle enabling us to map CNT defects with a resolution below 20 nm. These variations do not originate from topographic effects since the height over the CNT structure was fairly constant (see also Supporting Information). In this particular case, we also observed G-band intensity variations, which to our knowledge can have the following several

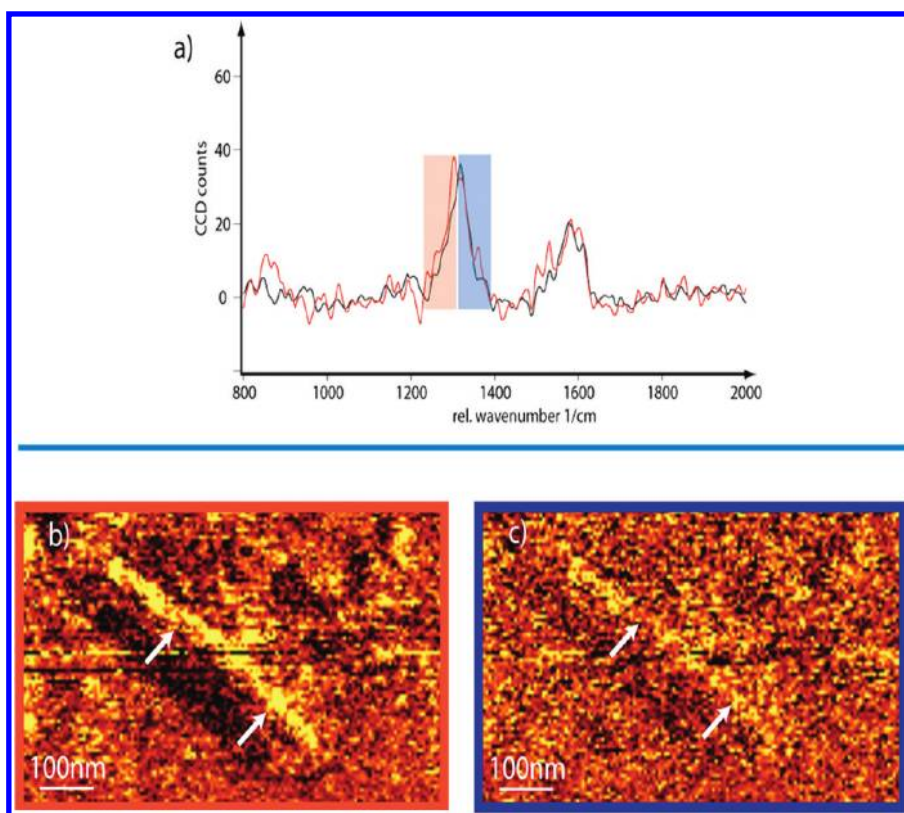


Figure 4. Fine structure mapping of CNTs. (a) Represents two Raman spectra taken at two different positions over a CNT. The D-mode's peak position varies over a range of ~ 20 wave numbers along the structure. The lower energy D peak marked with the orange square was mapped out in (b) whereas the higher energy peak (blue square) is shown in (c). The white arrows point out regions where the lower energy map seems to have low signal while the higher energy peak demonstrates stronger contrast in these regions.

possible causes: (1) influence of the tip forces; (2) multiwall CNTs with abundant structural variations along the CNT; (3) several chirality changes within a single-wall CNT (SWCNT); and (4) the presence of a bundle of SWCNTs.

The topographical height of the larger diagonally oriented CNT structure observed in Figure 3 is 3–4 nm, indicating either a multiwall CNT or a bundle of several SWCNTs. Unfortunately, due to the cutoff frequency of our dichroic mirror, we were not able to observe radial breathing modes, which would help discriminate between CNT types, however catalytic CVD growth typically produces SWCNTs. On the basis of our observation that variations in applied pressure did not significantly affect the G-mode intensity in our measurements, we rule out the influence of locally varying tip pressure on G-mode variations in the images. To make a clear assessment of chiral changes along a SWCNT,⁴⁶ observation of the spectral position of the breathing mode is necessary. However, the measured height rules out a single SWCNT. Also, the fact that the contrast changes multiple times along the CNT makes it unlikely that the variation is caused by SWCNT chirality changes. We therefore believe that the contrast changes are related to the existence of SWCNT bundles on the sample substrate.

Lateral optical resolution was determined from a line scan of the D-mode intensity variation along the top of a CNT structure (see inset Figure 3c). This approach avoids optical artifacts arising from convolution of optical response with the sample topography. There were no significant changes in CNT topography along this line (see also Supporting Information), demonstrating that the observed optical signal changes arise from

the intrinsic properties of the sample. Here, the D-mode line-scan shows a sharp decrease as well as an increase (see inset Figure 3c) with transition widths of 23 and 18 nm, respectively, leading us to estimate a lateral optical resolution ≤ 23 nm. Line scans over apparent catalyst particles that showed a D-mode signal due to initial growth of CNTs had an optical width of around 22 nm, comparable to the line scan along the CNT (see Supporting Information).

Hyperspectral imaging makes it possible to distinguish between shifts in peak position and in peak intensity, giving pixel-by-pixel insight into the local sample chemistry. In an attempt to illustrate this, we left the fresh CNT sample in ambient conditions for four days to heterogeneously “functionalize” the CNTs with random absorbates. This was motivated by the known changes in the D-mode peak position due to CNT functionalization by molecules, salts, and metallic nanoparticles.^{55,56} Indeed, after four days, we observed small, but statistically significant and spatially correlated position-dependent variations in the D-mode peak positions, as shown in Figure 4. In particular, the D-mode peak position ranged between 1302 and 1324 cm^{-1} along the CNT structure. In contrast, shifts in the G-band were spatially uncorrelated and apparently due to noise. We generated spectral maps splitting the D-mode intensity between two distinct spectral windows, 1259 to 1310 cm^{-1} (orange region in Figure 4a) and 1311 to 1350 cm^{-1} (blue area in Figure 4a), to visualize the effects of peak shifts. The subsequent maps showed marked, mostly anticorrelated, contrast (Figure 4b,c). To ensure that the observed difference was not simply an effect of overall intensity modulation as observed for the example shown in Figure 3,

we verified that the intensity of the peak is comparable along the CNT structure. It should also be noted that in the freshly prepared sample we did not observe systematic, spatially correlated shifts of the D-peak position.

In summary, we were able to reproducibly fabricate durable optically resonant coaxial antennae on the apex of scanning probes with an excellent yield. This geometry combines the spectroscopic advantages of coupled resonant optical antennae with the good AFM imaging properties of sharp tips. We showed that with this geometry we reproducibly achieve significant Raman signal enhancement on dielectric samples using linearly polarized light in a gap-mode-free imaging modality, enabling full Raman hyperspectral mapping pixel by pixel, independent of the substrate. As a proof of principle, we mapped the D and G mode intensities, as well as small variations in the D-mode peak position, for CNTs grown on fused silica. Furthermore, the coaxial structure ultimately enables excitation from the backside of the structure, to create background-free optical near fields at the tip apex while maintaining the polarization, which will be the subject of future work.

■ ASSOCIATED CONTENT

S Supporting Information. Experimental setup, resonance measurement of coaxial antennae, theoretical modeling, fabrication of coaxial antennae on SPM tip, topography-independent optical intensity variations, and additional figures. This material is available free of charge via the Internet at <http://pubs.acs.org>.

■ AUTHOR INFORMATION

Corresponding Author

*E-mail: (A.W.B.) afweber-bargioni@lbl.gov; (S.C.) scabrini@lbl.gov; (P.J.S.) pjschuck@lbl.gov.

Present Addresses

^{||}CEA, 17 Rue des Martyrs, 38054 Grenoble Cedex 9, France.

[†]Sandia National Laboratory Livermore, 7011 East Avenue Livermore, CA 94550.

■ ACKNOWLEDGMENT

The authors specifically thank Ed Wong for fast and high quality technical support, as well as our colleagues at the Molecular Foundry for stimulating discussion, advice, and assistance. This work was performed at the Molecular Foundry, Lawrence Berkeley National Laboratory, and was supported by the Office of Science, Office of Basic Energy Sciences, Scientific User Facilities Division, of the U.S. Department of Energy under Contract No. DE-AC02-05CH11231.

■ REFERENCES

- (1) Novotny, L.; Hecht, B. *Principles of Nano-Optics*; Cambridge University Press: New York, 2006.
- (2) Schuck, P. J.; Fromm, D. P.; Sundaramurthy, A.; Kino, G. S.; Moerner, W. E. *Phys. Rev. Lett.* **2005**, *94* (1), No. 017402–4.
- (3) Muhschlegel, P.; Eisler, H. J.; Martin, O. J. F.; Hecht, B.; Pohl, D. W. *Science* **2005**, *308* (5728), 1607–1609.
- (4) Wang, H.; Wu, Y.; Lassiter, B.; Nehl, C. L.; Hafner, J. H.; Nordlander, P.; Halas, N. J. *Proc. Natl. Acad. Sci. U.S.A.* **2006**, *103* (29), 10856–10860.
- (5) Vedantam, S.; Lee, H.; Tang, J.; Conway, J.; Staffaroni, M.; Yablonovitch, E. *Nano Lett.* **2009**, *9* (10), 3447–3452.

- (6) Kosako, T.; Kadoya, Y.; Hofmann, H. F. *Nat. Photonics* **2010**, *4* (5), 312–315.
- (7) Biagioni, P.; Huang, J. S.; Duo, L.; Finazzi, M.; Hecht, B. *Phys. Rev. Lett.* **2009**, *102* (25), No. 256801.
- (8) Zhang, Z.; Weber-Bargioni, A.; Wu, S. W.; Dhuey, S.; Cabrini, S.; Schuck, P. J. *Nano Lett.* **2009**, *9* (12), 4505–4509.
- (9) Olmon, R. L.; Rang, M.; Krenz, P. M.; Lail, B. A.; Saraf, L. V.; Boreman, G. D.; Raschke, M. B. *Phys. Rev. Lett.* **2010**, *105* (16), No. 167403.
- (10) Novotny, L. *Phys. Rev. Lett.* **2007**, *98* (26), No. 266802.
- (11) Hrelescu, C.; Sau, T. K.; Rogach, A. L.; Jackel, F.; Feldmann, J. *Appl. Phys. Lett.* **2009**, *94* (15), No. 153113.
- (12) Ghenuche, P.; Cherukulappurath, S.; Quidant, R. *New J. Phys.* **2008**, *10*, No. 105013.
- (13) Hicks, E. M.; Zou, S. L.; Schatz, G. C.; Spears, K. G.; Van Duyne, R. P.; Gunnarsson, L.; Rindzevicius, T.; Kasemo, B.; Kall, M. *Nano Lett.* **2005**, *5* (6), 1065–1070.
- (14) Rogobete, L.; Kaminski, F.; Agio, M.; Sandoghdar, V. *Opt. Lett.* **2007**, *32* (12), 1623–1625.
- (15) Murphy-DuBay, N.; Wang, L.; Kinzel, E. C.; Uppuluri, S. M. V.; Xu, X. *Opt. Express* **2008**, *16* (4), 2584–2589.
- (16) Matteo, J. A.; Fromm, D. P.; Yuen, Y.; Schuck, P. J.; Moerner, W. E.; Hesselink, L. *Appl. Phys. Lett.* **2004**, *85* (4), 648–650.
- (17) Wang, D. X.; Yang, T.; Crozier, K. B. *Opt. Express* **2010**, *18* (10), 10388–10394.
- (18) Fischer, H.; Martin, O. J. F. *Opt. Express* **2008**, *16* (12), 9144–9154.
- (19) Fleischer, M.; Stanciu, C.; Stade, F.; Stadler, J.; Braun, K.; Heeren, A.; Haffner, M.; Kern, D. P.; Meixner, A. J. *Appl. Phys. Lett.* **2008**, *93* (11), No. 111114.
- (20) Chang, S. W.; Chuang, S. L. *Opt. Lett.* **2009**, *34* (1), 91–93.
- (21) Kang, J. H.; Kim, D. S.; Park, Q. H. *Phys. Rev. Lett.* **2009**, *102* (9), No. 093906.
- (22) Li, K. R.; Stockman, M. I.; Bergman, D. J. *Phys. Rev. Lett.* **2003**, *91* (22), No. 227402.
- (23) Lim, D. K.; Jeon, K. S.; Kim, H. M.; Nam, J. M.; Suh, Y. D. *Nat. Mater.* **2010**, *9* (1), 60–67.
- (24) Kinkhabwala, A.; Yu, Z. F.; Fan, S. H.; Avlasevich, Y.; Mullen, K.; Moerner, W. E. *Nat. Photonics* **2009**, *3* (11), 654–657.
- (25) Camden, J. P.; Dieringer, J. A.; Wang, Y. M.; Masiello, D. J.; Marks, L. D.; Schatz, G. C.; Van Duyne, R. P. *J. Am. Chem. Soc.* **2008**, *130* (38), 12616.
- (26) Pettinger, B.; Ren, B.; Picardi, G.; Schuster, R.; Ertl, G. *Phys. Rev. Lett.* **2004**, *92* (9), No. 096101.
- (27) Neacsu, C. C.; Dreyer, J.; Behr, N.; Raschke, M. B. *Phys. Rev. B* **2006**, *73* (19), No. 193406–4.
- (28) Sackrow, M.; Stanciu, C.; Lieb, M. A.; Meixner, A. J. *Chem-PhysChem* **2008**, *9* (2), 316–320.
- (29) Deckert-Gaudig, T.; Deckert, V. *Small* **2009**, *5* (4), 432–436.
- (30) Stadler, J.; Schmid, T.; Zenobi, R. *Nano Lett.* **2010**, *10* (11), 4514–4520.
- (31) Taminiu, T. H.; Moerland, R. J.; Segerink, F. B.; Kuipers, L.; van Hulst, N. F. *Nano Lett.* **2007**, *7* (1), 28–33.
- (32) Farahani, J. N.; Pohl, D. W.; Eisler, H. J.; Hecht, B. *Phys. Rev. Lett.* **2005**, *95* (1), No. 017402.
- (33) Weber-Bargioni, A.; Schwartzberg, A.; Schmidt, M.; Harteneck, B.; Ogletree, D. F.; Schuck, P. J.; Cabrini, S. *Nanotechnology* **2010**, *21*, No. 065306.
- (34) Weber-Bargioni, A.; Schwartzberg, A.; Cornaglia, M.; Urban, J. J.; Ogletree, D. F.; Cabrini, S.; Schuck, P. J. Unpublished work.
- (35) Li, D.; Gordon, R. *Phys. Rev. A* **2010**, *82* (4), No. 041801(R).
- (36) Cattrysse, P. B.; Fan, S. H. *Appl. Phys. Lett.* **2009**, *94* (23), No. 231111.
- (37) Lockyear, M. J.; Hibbins, A. P.; Sambles, J. R.; Lawrence, C. R. *Phys. Rev. Lett.* **2005**, *94* (19), No. 193902.
- (38) Poujet, Y.; Salvi, J.; Baida, F. I. *Opt. Lett.* **2007**, *32* (20), 2942–2944.

- (39) de Waele, R.; Burgos, S. P.; Polman, A.; Atwater, H. A. *Nano Lett.* **2009**, *9* (8), 2832–2837.
- (40) Neacsu, C. C.; Berweger, S.; Olmon, R. L.; Saraf, L. V.; Ropers, C.; Raschke, M. B. *Nano Lett.* **2010**, *10* (2), 592–596.
- (41) De Angelis, F.; Das, G.; Candeloro, P.; Patrini, M.; Galli, M.; Bek, A.; Lazzarino, M.; Maksymov, I.; Liberale, C.; Andreani, L. C.; Di Fabrizio, E. *Nat. Nanotechnol.* **2010**, *5* (1), 67–72.
- (42) de Waele, R.; Burgos, S. P.; Atwater, H. A.; Polman, A. *Opt. Express* **2010**, *18* (12), 12770–12778.
- (43) Stockman, M. I. *Phys. Rev. Lett.* **2004**, *93* (13), No. 137404.
- (44) Ismach, A.; Segev, L.; Wachter, E.; Joselevich, E. *Angew. Chem., Int. Ed.* **2004**, *43* (45), 6140–6143.
- (45) Joselevich, E.; Lieber, C. M. *Nano Lett.* **2002**, *2*, 1137–1141.
- (46) Anderson, N.; Hartschuh, A.; Novotny, L. *Nano Lett.* **2007**, *7* (3), 577–582.
- (47) Hartschuh, A. *Angew. Chem., Int. Ed.* **2008**, *47* (43), 8178–8191.
- (48) Hartschuh, A.; Pedrosa, H. N.; Novotny, L.; Krauss, T. D. *Science* **2003**, *301* (5638), 1354–1356.
- (49) Yano, T.; Verma, P.; Saito, Y.; Ichimura, T.; Kawata, S. *Nat. Photonics* **2009**, *3* (8), 473–477.
- (50) Anderson, N.; Bouhelier, A.; Novotny, L. *J. Opt. A: Pure Appl. Opt.* **2006**, *8* (4), S227–S233.
- (51) Anger, P.; Bharadwaj, P.; Novotny, L. *Phys. Rev. Lett.* **2006**, *96* (11), No. 113002–4.
- (52) Hoppener, C.; Novotny, L. *Nanotechnology* **2008**, *19* (38), No. 384012.
- (53) Gerton, J. M.; Wade, L. A.; Lessard, G. A.; Ma, Z.; Quake, S. R. *Phys. Rev. Lett.* **2004**, *93* (18), No. 180801.
- (54) Stockle, R. M.; Suh, Y. D.; Deckert, V.; Zenobi, R. *Chem. Phys. Lett.* **2000**, *318* (1–3), 131–136.
- (55) Strano, M. S.; Dyke, C. A.; Usrey, M. L.; Barone, P. W.; Allen, M. J.; Shan, H. W.; Kittrell, C.; Hauge, R. H.; Tour, J. M.; Smalley, R. E. *Science* **2003**, *301* (5639), 1519–1522.
- (56) Qu, L. W.; Martin, R. B.; Huang, W. J.; Fu, K. F.; Zweifel, D.; Lin, Y.; Sun, Y. P.; Bunker, C. E.; Harruff, B. A.; Gord, J. R.; Allard, L. F. *J. Chem. Phys.* **2002**, *117* (17), 8089–8094.